High-Accuracy Structure of Cyclobutane by Femtosecond Rotational Raman Four-Wave Mixing

Dominique S. Kummli, Hans M. Frey, and Samuel Leutwyler*

Departement für Chemie und Biochemie, Universität Bern, Switzerland

Received: July 30, 2007; In Final Form: September 4, 2007

The femtosecond degenerate four-wave mixing (fs-DFWM) technique is applied for the measurement of accurate rotational constants of cyclobutane (C_4H_8). The vibrational levels of C_4H_8 exhibit tunneling splitting due to the ring-puckering interconversion between the symmetry-equivalent D_{2d} minima via a planar D_{4h} barrier. For the $v = 0$ ground state, the fs-DFWM method yields a rotational constant $B_0^+ = 10663.452(18)$ MHz. The ring-puckering tunneling leads to slightly different rotational constants for the 0^+ and 0^- levels, $B_0^+ - B_0^- = 33 \pm 2$ kHz. This difference increases by a factor of ~90 in the $v = 1^+/1^-$ ring-puckering states to $B_1^+ - B_1^- = -3059 \pm 4$ kHz. Combining the experimental rotational constants with the structure parameters and rotational constants calculated by high-level ab initio calculations allows us to determine accurate equilibrium and vibrationally averaged structure parameters for cyclobutane, for example, r_e(C−C) = 1.5474 Å, r_e(C−H$_{axial}$) = 1.0830 Å, r_e(C−H$_{equatorial}$) = 1.0810 Å, and ring puckering angle $\theta_e = 29.8°$.

I. Introduction

Time-resolved femtosecond degenerate four-wave mixing (fs-DFWM) can be applied as a Raman scattering type of rotational coherence spectroscopy (RCS).[1−3] This background-free rotational Raman technique[4−15] permits the determination of very accurate rotational and centrifugal distortion constants of the vibrational ground state,[16−18] and of low-lying thermally populated vibrational levels.[18] Following initial studies on nonpolar rigid molecules,[8,16,17,19] here we investigate cyclobutane (C_4H_8), which is a relatively rigid molecule with a single large-amplitude low-frequency mode. Cyclobutane has two equal-energy D_{2d} symmetric puckered equilibrium structures, shown in Figure 1. The equivalent minima are interconverted along the ring-puckering coordinate, with an intermediate barrier of ~500 cm^{-1} height[20−24] that corresponds to a planar D_{4h} symmetric structure. The symmetry of cyclobutane excludes a permanent dipole moment, and, as a consequence, no pure rotational spectrum can be observed.

Structural information on cyclobutane has been obtained from electron diffraction (ED) measurements,[25,26] from Raman[27] and infrared [20−22,28,29] spectroscopies and by Fourier transform microwave spectroscopy of mono- and dideuterated cyclobutane.[30,31] The earliest geometry parameters were measured by Dunitz and Schomaker and by Almenningen et al. using electron diffraction.[25,26] They obtained the C−C and C−H bond lengths but could not reliably determine the ring-puckering angle θ (see Figure 1). Lord and Stoicheff recorded the rotational Raman spectrum of C_4H_8 and determined the C−C bond length as 1.558(3) Å;[27] again, the puckering angle was not determined. Ueda and Shimanouchi analyzed an infrared difference band in the CH$_2$ symmetrical-stretching fundamental.[28] They fitted a double-minimum ring-puckering potential (see Figure 2) with a barrier height of 448 cm^{-1} and obtained an equilibrium angle $\theta = 33°$. Later, Stone, and Mills extended the infrared and Raman measurements on both C_4H_8 and C_4D_8.[20] They fitted a
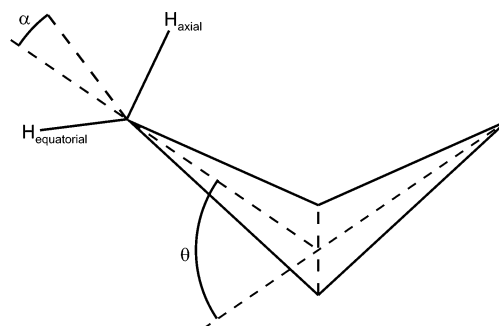

Figure 1. Schematic D_{2d} equilibrium structure of cyclobutane, with definition of the puckering angle θ, methylene rocking angle α, and the axial/ equatorial hydrogen atoms.
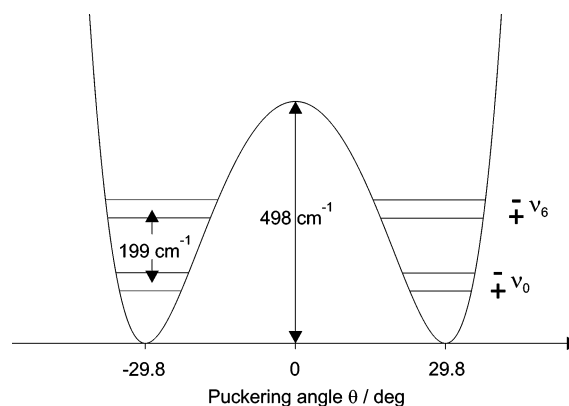

Figure 2. Schematic ν_6 ring-puckering potential of cyclobutane, showing the near-degenerate $v = 0^+/0^-$ and $\nu_6 = 1^+/1^-$ vibrational levels and parity labels. The puckering barrier is from ref 24, the equilibrium angle θ_e is that determined in this work.

modified puckering potential function with a barrier of 503 cm^{-1} and an equilibrium puckering angle $\theta_e = 34.3°$.[20] Malloy and Lafferty pointed out that there is a strong coupling between the angle θ and the CH$_2$ rocking angle α.[32] Egawa et al. obtained accurate structural parameters by combining electron diffraction

* Corresponding author. E-mail: leutwyler@iac.unibe.ch.

High-Accuracy Structure of Cyclobutane

J. Phys. Chem. A, Vol. 111, No. 46, 2007 **11937**

and Fourier-transform infrared (FTIR) spectroscopic measurements.[21] They included the CH_2 rocking deformation with an equilibrium angle $\alpha = 6°$ (see Figure 1) and proposed a new potential function in which the ring-puckering is coupled to the concerted CH_2 rocking motion.[22] Using a diode laser and high-resolution FTIR spectroscopy, Egawa et al. later determined rotational and centrifugal distortion constants for the $v = 0^+/0^-$ tunneling states and the $v_6 = 1^+/1^-$ level pair.[29] Li et al. recorded the color-center IR laser spectrum of cyclobutane in a supersonic molecular beam[33] and also obtained rotational constants of the $v = 0^+/0^-$ tunneling states.

Bauder and co-workers have measured the pure rotational spectra of the isotopomers cyclobutane-d_1 and cyclobutane-1,1-d_2 by pulsed microwave Fourier transform spectroscopy and obtained very accurate rotational constants.[30,31] A single D-substitution breaks the molecular symmetry; hence, cyclobutane-d_1 exists as an equatorial and an axial conformer. Their ring-puckering wave functions are localized due to the energy difference between the two wells that arises from the slightly different zero-point vibrational energy of the two conformers. In contrast, the cyclobutane-1,1-d_2 isotopomer has a symmetric double-minimum potential and undergoes ring-puckering tunneling between two equivalent forms. However, no microwave spectrum exists for cyclobutane itself.

An ab initio study of the structure, ring-puckering intrinsic reaction coordinate, and barrier height has been performed by Glendening and Halpern at the B3LYP, MP2, and CCSD(T) levels using basis sets up to quadruple-ζ.[23] Blake and Xantheas extended this recently to include MP4 calculations with large basis sets and calculated harmonic and anharmonic spectroscopic constants.[24] The complete basis set (CBS) extrapolations using the CCSD(T) method yielded barrier heights of 482 and 498 cm^{-1}, respectively.[23,24]

We report accurate rotational and centrifugal distortion constants of the ground and $v_6 = 1$ vibrational states of C_4H_8 using femtosecond time-resolved rotational Raman four-wave mixing (fs-FWM). The precision of the technique is high enough to determine separate rotational and centrifugal constants for the $(+)$ and $(-)$ tunneling components of the $v = 0$ and 1 levels of the ring-puckering vibration that are more accurate than previous determinations.[21,22,29] By combining our experimental data with an extrapolation technique[18] based on high-level ab initio calculations, including those of Blake and Xantheas,[24] we are able to calculate very accurate equilibrium and vibrationally averaged structure parameters of C_4H_8.

II. Experimental Section

The experimental setup employed for recording fs-DFWM spectra has been described earlier.[9,16] Briefly, the output of a MaiTai (Spectra Physics) Ti:sapphire oscillator is amplified with a Quantronix ODIN C femtosecond chirped-pulse amplifier (800 nm, 1000 Hz, 75 fs fwhm, 0.45 time bandwidth product, 12.63 nm bandwidth). The temporal and bandwidth properties of the femtosecond pulses were characterized with a single-shot second-harmonic-generation frequency-resolved optical gating device (Grenouille, Swamp Optics).

The probe beam runs over a retroreflector (1 in.) mounted on a computer-controlled 600-mm delay stage. The stage was constructed in-house and employs high-precision bearings and lead screw. Displacements are measured with a 500-mm glass ruler (Sony BL55-NEA) with a resolution of 100 nm. The optical delay line is enclosed in a vacuum-tight container and evacuated to $\leq 5 \times 10^{-2}$ mbar using a scroll pump (Varian Triscroll 300).[16] The two pump and the probe beams are focused

by a 1000-mm lens into a stainless-steel gas cell containing the sample. The generated four-wave mixing signal is detected by a cooled Hamamatsu H7422-50 photomultiplier. The signals were digitized with a LeCroy LT372 transient digitizer, scaled, combined, and stored in a PC.

Cyclobutane was synthesized in 55% yield via the Wolff–Kishner reduction of the carbonyl group of cyclobutanone[34] (ABCR GmbH, 98%). Measurements were performed at 15 mbar. The pressure was measured with an MKS Baratron capacitance gauge accurate to ± 0.1 mbar. The time delay is scanned in three overlapping regions (300, 370, and 270 ps) in steps of 33.3 fs. The energy of the laser was set to 15 μJ per beam. We were able to record 19 recurrences; the scan length was limited to 950 ps by the overall signal decay because of collisional dephasing. Increasing the laser power up to 100 μJ did not improve the signal-to-noise ratio.

III. DFWM Theory and Data Analysis

A. Vibrational and Rotational States and Level Populations. Simulations of fs-DFWM transients[16,17] as well as the underlying theory[35–37] are well established and are only briefly reviewed. Three polarized laser beams of equal intensity are focused in a forward box configuration into a Raman-active medium. Two pump pulses (E_1, E_2) induce an anisotropy by rotational Raman transitions in the medium. This anisotropy is probed via a third-order optical process. The probe beam (E_3) generates a four-wave mixing signal at times when the molecules are aligned. The time-dependent third-order polarization is given by

$$P^{(3)}(t) = E_3(t) \int_{-\infty}^{\infty} E_1(t)\, E_2$$
$$(t) \sum_N p_v \cdot p_{J,K} \cdot g_{J,K} \cdot g_{NS} \cdot b_{J'K'JK} \cdot e^{-k_{J,K'}} \cdot e^{i\Delta\omega_{J,K'}} \mathrm{d}t \quad (1)$$

involving a sum over the N populated levels. The squared norm of the third-order polarization, $|P^{(3)}(t)|^2$ (together with eq 1 in combination with level dependent transition probabilities) leads to the transient recorded.

Vibrational population factor p_v: Because we recorded our spectra at $T = 295$ K, the $v_6 = 1$ and 2 puckering levels at 199 and 398 cm^{-1} (Figure 2) are thermally populated with relative contributions of $p_{v_6=1} = 23\%$ and $p_{v_6=2} = 9.4\%$, respectively. The isolated contributions to the DFWM signal from the $v_6 = 1$ and 2 levels would be on the order of 5.3% and 0.9%, respectively. Note, however, that because the DFWM signal is proportional to the square modulus of $P^{(3)}(t)$ the contributions from the $v_6 = 1$ and 2 levels do not simply add into the total signal but give rise to interference terms with the dominant $v = 0$ DFWM signal, as is shown in Section IV.

The initial population of the rotational levels, $p_{J,K}$ in eq 1, is determined via the Boltzmann distribution by the rotational term values $E_{J,K}$ (see eq 2) and the sample temperature T. We fitted the $E_{J,K}$ according to the standard oblate symmetric top formula including quartic centrifugal distortion terms, note the v-dependence of the constants:

$$E_{J,K} = B_v\, J(J+1) - D_{J,v}\, J^2(J+1)^2 - D_{JK,v}\, J(J+1)K^2 -$$
$$D_{K,v}\, K^4 \quad (2)$$

For symmetric rotors, the M_J spatial degeneracy is $g_{K,M_J} = (2J+1)$ for the $K = 0$ states and $g_{K,M_J} = 2(2J+1)$ for those with $K \neq 0$. As a consequence of the low tunneling barrier to the ring puckering motion, $(+)/(-)$ pairs of puckering levels

TABLE 1: Nuclear Spin (NS) Irreducible Representations, Γ_{NS}, and Corresponding Statistical Weights, g_{NS}, for Cyclobutane (C_4H_8) in the MS Group D_{4h} for a_{1g} and b_{2u} Vibrational Levels

rotational state	Γ_{NS}: g_{NS} a_{1g} level[a]	Γ_{NS}: g_{NS} b_{2u} level[b]
$K = 0$, J even	A_{1g}: 43	B_{2u}: 33
$K = 0$, J odd	A_{2g}: 27	B_{1u}: 33
$K = 4p$	$[A_{1g} + A_{2g}]$: 70 (43 + 27)	$[B_{1u} + B_{2u}]$: 66 (33 + 33)
$K = 4p \pm 1$	E_g: 60	E_u: 60
$K = 4p \pm 2$	$[B_{1g} + B_{2g}]$: 66 (33 + 33)	$[A_{1u} + A_{2u}]$: 70 (43 + 27)

[a] $\nu_6 = 0^+$, 1^+, ... [b] $\nu_6 = 0-$, 1^-, ...

arise in the ν_6 vibration, see Figure 2. The rotational and centrifugal constants differ very slightly for the (+) and (−) member of each pair.

Because of the puckering tunneling, the nuclear spin states of $^{12}C_4H_8$ have to be treated in the molecular symmetry group D_{4h}.[33,38] The nuclear spin irreducible representations Γ_{NS} and statistical weights, g_{NS} in eq 1, can be evaluated for the individual vibrational−rotational states using the method given by Weber;[39] see also ref 38. Li et al. have previously given g_{NS} for the a_{1g} levels ($\nu_6 = 0^+$, 1^+, 2^+, ...);[33] however, the (−) tunneling levels ($\nu_6 = 0^-$, 1^-, 2^-, ...) transform as b_{2u}. For convenience, the g_{NS} are given for the a_{1g} and b_{2u} levels in Table 1.

The rotational Raman intensities for anisotropic Raman scattering, $b_{J'K'}^{JK}$ in eq 1, are described with the Clebsch−Gordan formalism[40] and are included according to Weber[41] for the O, P, R, and S transitions. The time bandwidth product of the fs laser has two distinct effects on the transient: (i) The transient has to be convoluted with the three fs laser pulse widths. The zero-time peak of Ar directly yields this as an apparatus function. (ii) The Raman processes are limited to transitions within the spectral bandwidth of the laser.

B. Rotational Energy Transfer. The initial population of the rotational levels at time delay $t = 0$ is given by the temperature of the sample. However, following the pump pulses at $t = 0$, the rotational coherence of the sample is destroyed slowly because of R → R and R → T rotational-state or -phase changing collisions. This dephasing is accounted for by the factor $e^{-k_{J,K}t}$ in eq 1, which is modeled according to the energy gap law model for collisional rotational energy transfer (RET).[42,43] In this model, the dephasing rate of a given rotational state is $k_{J,K} = a \cdot e^{-c\Delta E_{J,v}}$, where a and c are coefficients to be fitted, $\Delta E_{J,v} = |E_{J,v\pm 1} - E_{J,v}| = 2B_v J$ is the rotational level spacing and B_v is the rotational constant.[42,43] We considered transitions

with $\Delta J = \pm 1$ because including larger ΔJ transitions did not improve the fit. The procedure was validated by fitting the temperature T, which resulted in values within ± 10 K from the experimental $T = 295$ K. This model has been applied successfully for cyclopropane.[17]

C. Fitting. The fitting procedure employs a Levenberg−Marquardt least-squares fit and is written in the IDL language (RSI, Inc.). The evaluation of the transient according to eq 1 is highly parallelizable and was distributed over several processors with a shared library written in C under the OPENMP protocol. The fit was performed with a total of 13 free variables: the variables listed in Table 2, the amplitude and vertical offset of the transient, the background term, the temperature, the collisional dephasing coefficients a and c.[16] We started with values obtained from our ab initio calculations for the variables in Table 2, J_{max} fixed to 90, and the bandwidth of the laser to 155 fs.

IV. Results

A. Rotational Constants. Figure 3 shows an overview of the RCS transient of C_4H_8 recorded with Raman femtosecond degenerate four-wave mixing. The large Kerr-effect signal at time zero is off the scale of Figure 3 and is not shown. There is a rotational Raman contribution to the signal near time zero that provides information on the rotational constants,[5] but the information is much less accurate than that obtained from the later transients. In Figure 3, the exponential decay of the signal can be seen. This arises from collisional dephasing of the rotational states, see Section III, and is fitted using the energy gap law model.[17,42,43] With increasing delay time, each of the rotational coherences shows increasing spread. This is due to the effect of centrifugal distortion on the rotational energies, the higher-J rotational states giving signal contributions at later delay than the low-J states.

Figure 4 shows more detailed views of three recurrences (13, 13.5, 14) at medium delay and three recurrences (17, 17.5, and 18) at late delay. As compared to recurrences 1−5 in Figure 3, the medium and late coherences exhibit an extensive structure that yields detailed information on the rotational and centrifugal constants. In the integer recurrences, interference occurs between the transitions with $\Delta J = \pm 2$ and $\Delta J = \pm 1$, with different Clebsch−Gordan coefficients, whereas the half-integer recurrences involve $\Delta J = \pm 2$ transitions only. Hence, the half-integer recurrences (13.5 and 17.5) are less complex than the integer coherences (13, 14, 17, 18) in Figure 4.

Additional contributions arise from the different *vibrational* states: The early part of each recurrence in Figure 4 arises from

TABLE 2: Experimental and Calculated Rotational (MHz) and Centrifugal Distortion (kHz) Constants of Cyclobutane ($^{12}C_4H_8$)

parameter	femtosecond DFWM[a]	Fourier-transform IR[b]	color-center IR laser[c]	MP2/cc-pVTZ anharmonic[d]	MP2/cc-pVDZ anharmonic[a]
			$v = 0$ state		
B_0^+	10 663.452(18)	10 664.5(6)	10 666.9(15)	10 671.56	10 527.12
ΔB_0^e	0.033(2)	0.3(11)	0.7(17)		
D_J	5.541(11)	5.64(2)		5.7043	5.3782
ΔD_J	0.0[f]	0.04(60)			
D_{JK}	−8.218(36)	6.9(84)		−7.2181	−6.7889
			ν_6, $v = 1$ state		
B_1^+	10 643.199(80)	10 644.4(27)		10 653.03	10 508.88
ΔB_1^e	−3.059(4)	−4.2(52)			
D_J	5.959(52)	4.5(27)			
ΔD_J	0.0[f]	−5.4(77)			
D_{JK}	−8.218(36)[g]				
J_{max}	90	15	7		

[a] This work. [b] Reference 29. [c] Reference 33. [d] Reference 24. [e] $\Delta B_v = B_v^+ - B_v^-$. [f] Constrained to zero. [g] Fixed to $v = 0$ value.

High-Accuracy Structure of Cyclobutane

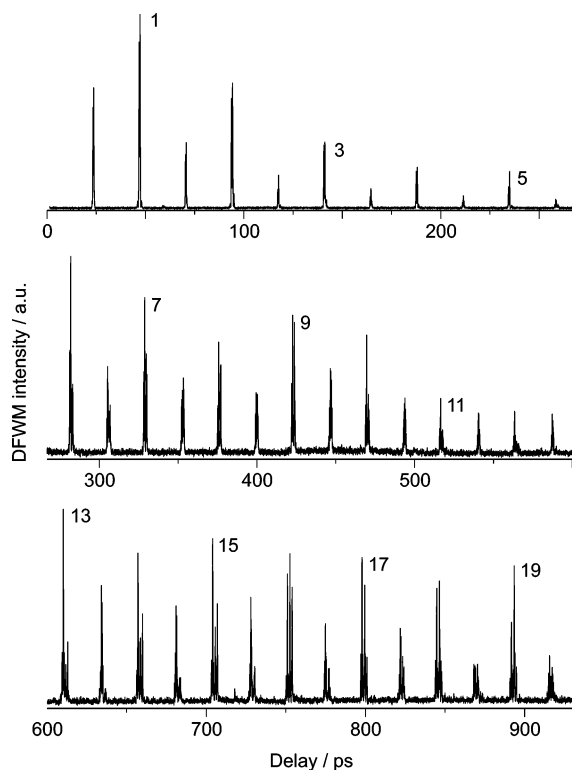*J. Phys. Chem. A, Vol. 111, No. 46, 2007* **11939**

Figure 3. Femtosecond degenerate four-wave mixing (fs-DFWM) rotational coherence transient of cyclobutane in a gas cell (298 K, $p =$ 15 mbar), using 75-fs pulses at 800 nm. The numbers refer to integer coherences.
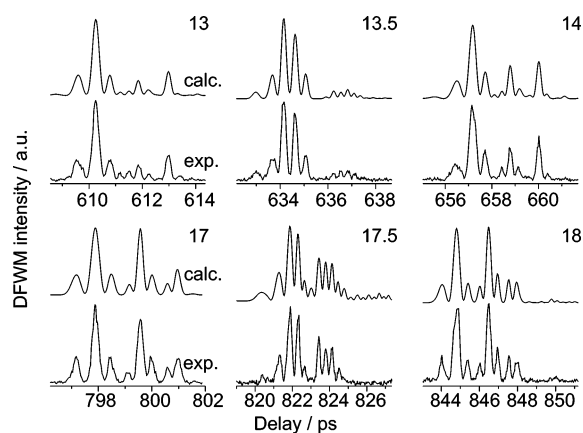

Figure 4. Six individual integer and half-integer fs-DFWM rotational recurrences 13, 13.5, 14, 17, 17.5, and 18 of cyclobutane from experiment (lower traces, enlarged from Figure 3) and calculation (upper traces), at medium and late delay times.

the $v = 0$ ground state, whereas the $v_6 = 1$ state has a slightly smaller rotational constants and contributes to each recurrence at later time. Figure 5 shows in detail the effect of the $v_6 = 1$ vibrational contribution on the 14.5 rotational recurrence: The $v = 0$ state, Figure 5a, yields a calculated recurrence with a maximum peak at 681.1 ps. The $v_6 = 1$ state, Figure 5b, by itself gives a calculated recurrence that peaks at 682.2 ps. Note that the $P^{(3)}(t)$ terms of the $v = 0$ and 1 levels add coherently in eq 1 and the square modulus $|P^{(3)}(t)|^2$ is taken afterward. This leads to destructive interference between the two vibrational contributions from 682 to 683 ps and constructive interference from 683 to 684 ps, as shown by the calculated recurrence Figure 5c. This agrees with the experimental rotational coherence in Figure 5d. In analogy to Figure 4, the entire transient
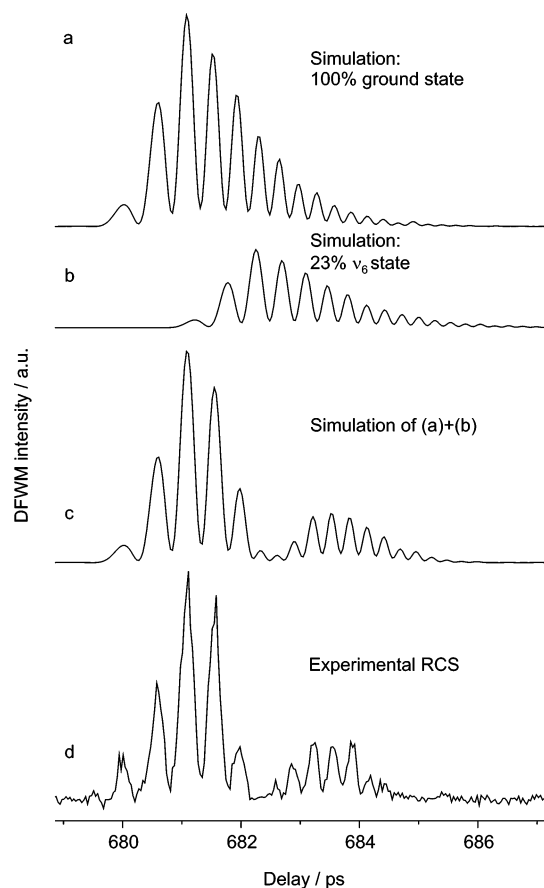

Figure 5. Effect of the thermally excited v_6 vibrational state on the half-integer fs-DFWM recurrence no. 14.5 of cyclobutane: (a) calculated with only $v = 0^+/0^-$ population of 100%, (b) with only the $v_6(v = 1^+/1^-)$ population of 23%, (c) coherent addition of a and b, note the interference arising from the addition of the $v = 0$ and $v_6 = 1$ contributions, (d) experimental fs-DFWM recurrence.

can be fitted in great detail. The rotational and centrifugal constants obtained are given in Table 2.

The tunneling splitting between the 0^+ and 0^- vibrational ground states of cyclobutane has not been measured directly because the v_6 ring-puckering mode is neither IR nor Raman active. However, several groups have observed the ground-state combination differences for the v_6 tunneling levels in the sidebands of various infrared (IR) bands, for example, the v_{14} and v_{16} bands.[20-22,28,29] From a fit of these v_6 combination differences to one-dimensional puckering function containing quadratic, quartic, and sextic terms, Egawa et al. calculated a ∼300 MHz tunneling splitting between the $0^+/0^-$ states.[21] Using the same type of puckering potential and an ab initio calculated IRC potential curve, Glendening and Halpern obtained a $0^+/0^-$ splitting of ∼360 MHz.[23]

Caminati et al. have observed the effect of the puckering tunneling on the B_0 rotational constant in the Fourier-transform microwave spectrum of the cyclobutane-1,1-d_2 isotopomer.[31] They determined the difference between the B_0^+ and B_0^- rotational constants as $-35(\pm 7)$ kHz and that between C_0^+ and C_0^- as $+10(\pm 7)$ kHz.[31] The effect of the tunneling on the A_0 rotational constant was predicted to be 1 kHz, smaller than the experimental error.[31] They simultaneously fitted these differences of rotational constants and the puckering level IR combination differences from ref 21, obtaining an effective coupled ring-puckering/CH$_2$ rocking potential valid for the combined rotational and vibrational measurements on the C$_4$H$_8$, C$_4$H$_6$D$_2$, and C$_4$D$_8$ isotopomers. They calculated $0^+/0^-$ vibra-

TABLE 3: Vibrationally Averaged (r_0, r_z) Structure Parameters of Cyclobutane (Distances in Å, Angles in Degrees)

parameter	r_0 fs-DFWM/ CCSD(T)/cc-pVXZ[a]	r_0 micro- wave[b]	r_z electron diffraction[c]	r_0 MP2 cc-pVTZ[d]
$r(C−C)$	1.5562	1.5549(5)	1.552(1)	1.554
$r(C−H)_{axial}$	1.0888	1.0934(19)	1.093(3)[e]	1.095
$r(C−H)_{equatorial}$	1.0865	1.0910(9)		1.093
$\angle HCH$	109.04	109.33(14)	106.4(13)	109.03
$\angle CCC$	88.18	88.23(3)	88.3(2)	87.89
θ	28.92	28.32(23)	27.9(16)	30.90

[a] This work. [b] For cyclobutane-d_1, cyclobutane-1,1-d_2; refs 30 and 31. [c] r_z distances; ref 21. [d] Reference 24. [e] $r(C−H)_{axial}$ is assumed to be equal to $r(C−H)_{equatorial}$.

TABLE 4: Equilibrium (r_e) Structure Parameters of Cyclobutane (Distances in Å, Angles in Degrees)

parameter	r_e fs-DFWM[a] CCSD(T)/cc-pVXZ	r_e CCSD(T) cc-pVQZ[b]	r_e CCSD(T) cc-pVTZ[c]	r_e CCSD(T) aug-cc-pVTZ[c]
r(C−C)	1.5474	1.550	1.5524	1.5535
r(C−H)$_{axial}$	1.0830	1.091	1.0920	1.0929
r(C−H)$_{equatorial}$	1.0810	1.089	1.0901	1.0910
$\angle HCH$	109.24	109.07	109.13	109.15
$\angle CCC$	88.04	88.07	88.00	88.06
θ	29.79	29.59	30.11	29.68

[a] This work. [b] Reference 23. [c] Reference 24.

tional level splittings of 228 ± 9 MHz for C_4H_8, 95 ± 4 MHz for 1,1-d_2-cyclobutane, and 5.7 ± 0.2 MHz for C_4D_8.[31] Egawa et al. have also fitted separate rotational constants for the $\nu = 0^+/0^-$ and the $\nu_6 = 1^+/1^-$ levels.[29] However, the fitted differences $\Delta B_0 = B_0^+ - B_0^-$ and $\Delta B_1 = B_1^+ - B_1^-$ are about five and two times smaller than the respective 1σ standard deviations of their fit (see Table 2). Also, their fitted ΔB_0 of 300 kHz[21] is nine times larger than that measured by Caminati et al. for cyclobutane-1,1-d_2.[31] From the above, it is seen that the effect of the puckering tunneling on the B_0 constant can be measured only if the rotational constants are measured with accuracy in the kHz range.

To constrain the number of free parameters in the fit, we initially fixed the ΔB_0 difference to 35 kHz, the value for cyclobutane-1,1-d_2.[31] Similarly, the ΔB_1 difference for the ν_6 $\nu = 1$ state was fixed to -4.2 MHz, as given by Egawa et al.[29] With these constraints, our fit converges to B_0 and B_1 values that are consistently 0.011% or 1.2 MHz smaller than those given by Egawa et al., as given in Table 2. Also, our D_J values converge to values about 4% smaller than those of Egawa et al., see Table 2. These differences arise because our experiment reproduces the entire room-temperature thermal population up to $J = 90$, whereas Egawa et al. fitted transitions only up to $J = 15$ and Li et al. up to $J = 7$.[29,33]

Two additional fits were performed to determine only the tunneling splitting. In the first fit, all rotational and centrifugal constants were fixed at their converged values, except for the rotational constant of the $\nu = 0^-$ level. We obtain $B_0^- = 10663.4192(2)$ MHz, which is 33 ± 2 kHz smaller than B_0^+. This is in good agreement with the analogous difference measured for cyclobutane-1,1-d_2, which is 35 ± 7 kHz.[31] In the second fit, only B_1^- was allowed to vary, which resulted in $\Delta B_1 = -3.059$ MHz; note that B_1^- is larger than B_1^+. This tendency was also observed by Egawa et al., who obtained a difference of -4.2 ± 5.9 MHz.[29]

The centrifugal constants $D_{J,0}$ and $D_{JK,0}$ could be determined to within ±11 and ±36 kHz (1σ), respectively, which is one to 2 orders of magnitude more accurate than those in previous work.[29,30] The signs and magnitudes of D_J and D_{JK} are consistent with the Δ_J and Δ_{JK} centrifugal constants of the cyclobutane-d_1 isotopomer[30] and also with those of the anharmonic ab initio calculations.[24]
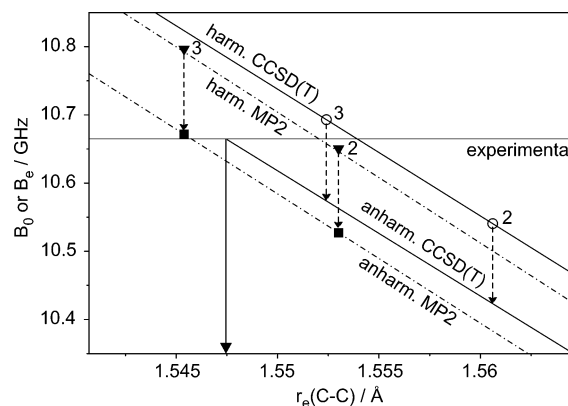

Figure 6. Ab initio equilibrium rotational constants B_e calculated with the MP2 and CCSD(T) methods plotted vs the $r_e(C−C)$ bond length, using the cc-pVDZ and cc-pVTZ basis sets (marked as 2, 3). Also shown are the MP2 vibrationally averaged B_0 constants. The dot−dashed lines connect the MP2 values; the full lines connect the CCSD-(T) equilibrium values. The vertical dashed arrows show the effect of vibrational averaging on the B_e constants at the MP2 level; this shift is transferred to the CCSD(T) level, where no vibrationally averaged B_0 values are available. The experimental B_0 is drawn as a horizontal line.

B. Molecular Structure. An overview of vibrationally averaged (r_0, r_z) structure parameters of cyclobutane determined previously and in this work is given in Table 3. Although calculations of vibrationally averaged structures would be desirable at the CCSD(T) level, they are currently beyond computational reach. Hence, we adopted the procedure previously applied for CS_2,[17,18] which combines (i) complete basis set (CBS) extrapolation of (ii) MP2 vibrationally averaged rotational constants to the experimental rotational constant using (iii) a CCSD(T) correction.

We begin with the equilibrium structure parameters and rotational constants, B_e and C_e of cyclobutane calculated at the MP2 and CCSD(T) levels using the cc-pVXZ ($X = 2, 3$) basis sets.[24] Figure 6 plots these B_e values versus the respective calculated equilibrium C−C distances, $r_e(C−C)$. The CCSD-(T) corrections, that is, the *differences* of the CCSD(T) and MP2 equilibrium rotational constants are denoted $\Delta B_e = B_e$ [CCSD-(T)] $- B_e$ (MP2). Note that the CCSD(T) and MP2 lines run very closely parallel, the CCSD(T) correction being $\Delta B_e = +32.5$ MHz.

High-Accuracy Structure of Cyclobutane

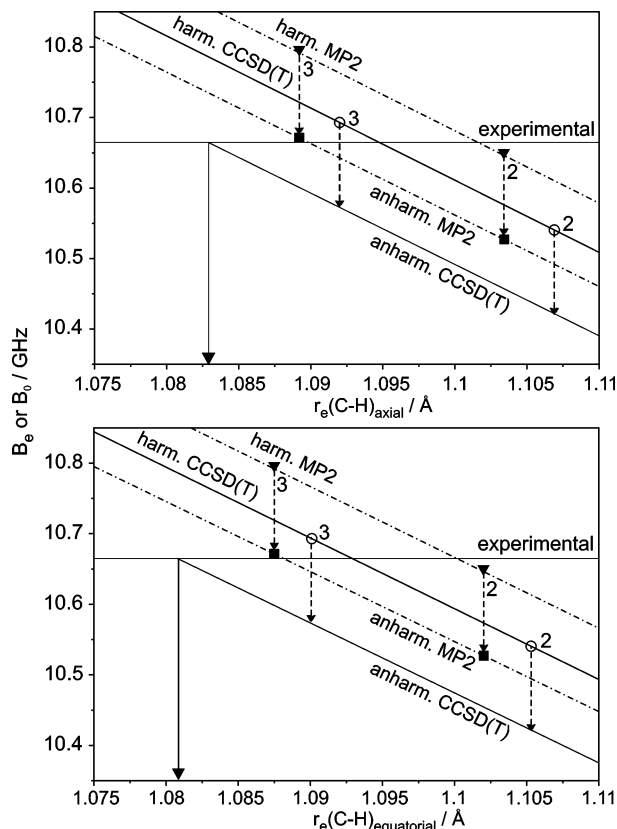*J. Phys. Chem. A, Vol. 111, No. 46, 2007* **11941**

Figure 7. Ab initio calculated rotational constants B_e from MP2 and CCSD(T) calculations and B_0 from MP2 calculations, plotted vs the calculated C−H$_{axial}$ and C−H$_{equatorial}$ equilibrium bond lengths. The dashed lines connect the MP2 values calculated with the cc-pVDZ and cc-pVTZ basis sets (marked as 2, 3). The full line connects the analogous CCSD(T) B_e values, the effect of vibrational averaging on the B_e constants is transferred from the MP2 to the CCSD(T) level, cf. Figure 6. The experimental B_0 is drawn horizontally.

Given the ab initio intramolecular force field, the effects of vibrational averaging can be treated computationally by second-order perturbation theory.[44−46] Previous experience shows that vibrational averaging effects are estimated reliably at the MP2 level.[17,18] Blake and Xantheas have calculated the MP2/cc-pVTZ vibrationally averaged B_0 and C_0 constants of cyclobutane,[24] which we have complemented with the analogous MP2/cc-pVDZ calculation. The MP2 B_0 constants are also indicated in Figure 6; note that the vibrational averaging decreases the B rotational constant by ∼120 MHz, as indicated by vertical arrows in Figure 6.

Finally, the vibrationally averaged CCSD(T) constants are estimated by combining the CCSD(T) correction ΔB_e with the MP2 vibrationally averaged B_0 constants, $B_0[CCSD(T)] \approx B_0$-(MP2) $+ \Delta B_e$, see Figure 6. The experimental B_0 is drawn horizontally in Figure 6; the difference between the B_0^+ and B_0^- constants is smaller than the width of the lines. The $B_0[CCSD$-(T)] line extrapolates to intersect the experimental B_0 line at $r_e(C−C) = 1.5474$ Å, with an estimated error of ± 0.0001 Å. Figure 7 shows the analogous plots for the C−H$_{axial}$ and C−H$_{equatorial}$ bond lengths. From the intersections of lower full lines as estimates for $B_0[CCSD(T)]$ with the horizontal $B_{0,exp}$ line we derive $r_e(C−H_{axial}) = 1.0830(2)$ Å and $r_e(C−H_{equatorial}) = 1.0810(2)$ Å.

The analogous plot for the angle θ brings out the effect of including correlation at the CCSD(T) level. As noted by Blake and Xantheas, θ_e decreases by 2° when going from the MP2 to the CCSD(T) level.[24] Note the relatively large difference
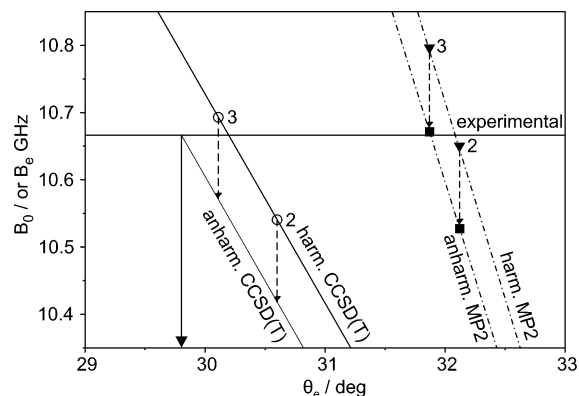

Figure 8. Ab initio calculated rotational constants B_e from MP2 and CCSD(T) calculations and B_0 from MP2 calculations, plotted vs the calculated equilibrium ring-puckering angle θ_e. See also Figures 6 and 7.
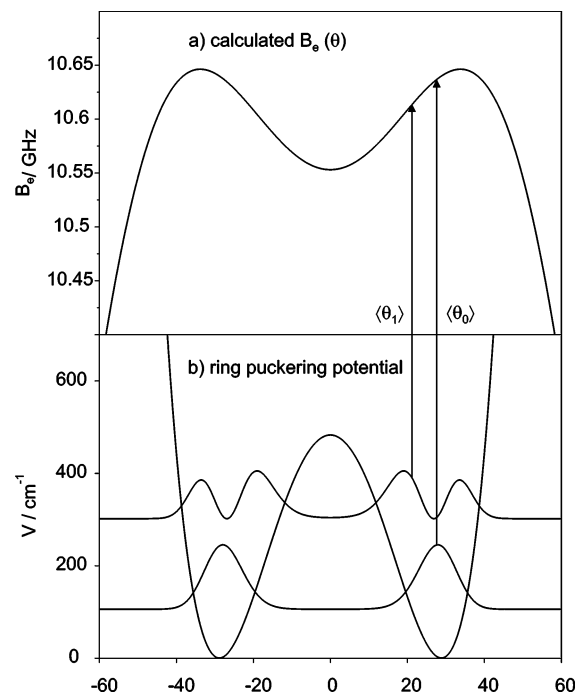

Figure 9. (a) MP2/cc-pVDZ calculated rotational constant B_e as a function of puckering angle θ. (b) Ring-puckering potential $V(\theta)$, with superimposed probability distributions $|\psi_v|^2$ of the $v = 0$ (full line) and $v = 1$ (dotted) puckering vibrations ν_6. The vertical arrows schematically indicate the decrease of the vibrationally averaged angle $\langle \theta_v \rangle$ with increasing vibrational excitation in the ring-puckering mode ν_6.

between the calculated MP2 and CCSD(T) θ angles and the steep angle dependence of B_0 as a function of θ. The extrapolated θ_e is 29.8°.

C. Ring-Puckering Dynamics. Beyond the equilibrium ring-puckering angle θ, the tunneling dynamics along the ring-puckering coordinate has been at the focus of interest of both experimental and theoretical studies for many years.[21,22,30−32,47] Malloy and Lafferty reported puckering angles of 29−37° for C$_4$H$_8$ and discussed the difficulty of determining θ from vibrational spectra. Egawa et al. determined a vibrationally averaged puckering angle $\theta_0 = 27.9 \pm 1.6°$ from a combination of electron diffraction and high-resolution IR spectroscopy. From the analyses of the microwave spectra of cyclobutane-d_1, the Bauder group reported a vibrationally averaged puckering angle $\theta_0 = 28.58 \pm 0.09°$,[30] and for cyclobutane-1,1-d_2 of $\theta_0 = 29.55 \pm 0.03°$.[31] Champion et al.[47] calculated the changes of molecular

structure along the puckering path at the SCF 4-31G(d,p) level and used a semirigid bender model to fit the observed infrared and Raman frequencies and rotational constants of the deuterated cyclobutanes;[30,31] they obtained a slightly larger angle and wider confidence interval, $\theta_0 = 30.0 \pm 1.5°$.

Figure 9b shows that the vibrational averaging along the ν_6 ring-puckering coordinate decreases θ relative to the equilibrium angle θ_e because of the strong asymmetry of the ring-puckering double-minimum potential.[21,31] At the MP2/cc-pVTZ level, $\theta_e - \theta_0$ is calculated to be $0.9°$.[24] Figure 9a shows that the calculated B_e constant as a function of θ goes through a maximum that fortuitously lies close to θ_e. Because θ decreases because of vibrational zero-point averaging and more so upon excitation of the ν_6 mode, B also decreases. The measured decrease from $v = 0$ to $v = 1$, $B_0^{obs} - B_1^{obs}$, is 20.25 MHz (Table 2), which is in good agreement with the MP2/cc-pVTZ predicted decrease $B_0^{calc} - B_1^{calc} = 18.45$ MHz.[24] This also rationalizes that the B_0^- rotational constant is slightly smaller than B_0^+. We note, however, that B_1^- is larger than B_1^+ (Table 2), contrary to expectation. It would be interesting to calculate the detailed effect of excitation in the ν_6 mode in terms of a semirigid bender model.[47]

V. Conclusions

The rotational and centrifugal constants of cyclobutane, C_4H_8, have been measured accurately using femtosecond rotational Raman coherences, detected by degenerate four-wave mixing. Rotational coherence transients of the $v = 0$ vibrational ground state and the ν_6 ($v = 1$) excited vibrational state have been recorded over a total delay time of 950 ps. The analysis yields the rotational constants with a relative accuracy of $\sim 2 \times 10^{-6}$. This about 30 times more accurate than that obtained by high-resolution Fourier transform infrared spectroscopy[29] and similar to the accuracy achieved by microwave spectroscopy for two deuterated isotopomers of cyclobutane.[30,31]

The ring-puckering inversion leads to a doubling of all vibrational states, leading to slight differences of the rotational constants B_0 and B_1 ($\nu_6 = 1$). These differences were measured to be $B_0^+ - B_0^- = 33 \pm 2$ kHz and $B_1^+ - B_1^- = -3059 \pm 4$ kHz, respectively. This shows the potential of the fs-DFWM method for high-accuracy measurements of rotational constants.

We have also performed ab initio MP2 calculations of the equilibrium and vibrationally averaged structural parameters and rotational constants, using the cc-pVXZ ($X = 2,3$) basis sets. In combination with the results of previous ab initio calculations,[23,24] it was possible to improve the MP2 values using the nearly constant difference of the *equilibrium* CCSD(T) and MP2 B_e constants and thereby correct the vibrationally anharmonic MP2 B_0 constants to CCSD(T) quality. The combination of an extrapolation procedure to the experimental B_0 allows us to determine the r_e structural parameters of cyclobutane to very high accuracy.

References and Notes

(1) Felker, P. M.; Zewail, A. H. *J. Chem. Phys.* **1987**, *86*, 2460.
(2) Felker, P. M. *J. Phys. Chem.* **1992**, *96*, 7844.

(3) Felker, P. M.; Zewail, A. H. Rotational Coherence Spectroscopy. In *Femtosecond Chemistry*; Manz, J.; Wöste, L., Eds.; VCH: Weinheim ,1995; Vol. I.
(4) Frey, H. M.; Beaud, P.; Gerber, T.; Mischler, B.; Radi, P. P.; Tzannis, A. P. *Appl. Phys. B* **1999**, *68*, 735.
(5) Brown, E. J.; Zhang, Q.; Dantus, M. *J. Chem. Phys.* **1999**, *110*, 5772.
(6) Lang, T.; Frey, H. M.; Beaud, P.; Motzkus, M. In *Raman Spectroscopy*; Zhang, S.-L.; Zhu, B.-F., Eds.; Wiley: New York, 2000.
(7) Lang, T.; Beaud, P.; Frey, H. M.; Motzkus, M. *J. Chem. Phys.* **2001**, *115*, 5418.
(8) Frey, H. M.; Beaud, P.; Gerber, T.; Mischler, B.; Radi, P. P.; Tzannis, A. P. *J. Raman Spectrosc.* **2000**, *31*, 71.
(9) Frey, H. M.; Müller, A.; Leutwyler, S. *J. Raman Spectrosc.* **2002**, *33*, 855.
(10) Frey, H. M.; Beaud, P.; Lang, T.; Motzkus, M. In *Femtochemistry and Femtobiology, Ultrafast Dynamics in Molecular Science*; Douhal, A.; Santamaria, J., Eds.; World Scientific Publishing: Singapore, 2002.
(11) Jarzeba, W.; Matylitsky, V. V.; Weichert, A.; Riehn, C. *Phys. Chem. Chem. Phys.* **2002**, *4*, 451.
(12) Matylitsky, V. V.; Jarzeba, W.; Riehn, C.; Brutschy, B. *J. Raman Spectrosc.* **2002**, *33*, 877.
(13) Jarzeba, W.; Matylitsky, V. V.; Riehn, C.; Brutschy, B. *Chem. Phys. Lett.* **2003**, *368*, 680.
(14) Riehn, C.; Matylitsky, V.; Jarzeba, W.; Brutschy, B.; Tarakeshwar, P.; Kim, K. *J. Am. Chem. Soc.* **2003**, *125*, 16455.
(15) Riehn, C.; Matylitsky, V. V.; Gelin, M. F. *J. Raman Spectrosc.* **2003**, *34*, 1045.
(16) Kummli, D.; Frey, H. M.; Keller, M.; Leutwyler, S. *J. Chem. Phys.* **2005**, *123*, 054308.
(17) Kummli, D.; Frey, H. M.; Leutwyler, S. *Chimia* **2006**, *60*, 212.
(18) Kummli, D.; Frey, H. M.; Leutwyler, S. *J. Chem. Phys.* **2006**, *124*, 144307.
(19) Frey, H.-M.; Kummli, D.; Keller, M.; Leist, R.; Leutwyler, S. In *Femtochemistry and Femtobiology*; Martin, M. M., J. T. Hynes, Eds.; Elsevier: Amsterdam, 2004.
(20) Stone, J. M. R.; Mills, I. M. *Mol. Phys.* **1970**, *18*, 631.
(21) Egawa, T.; Fukuyama, T.; Yamamoto, S.; Takabayashi, F.; Kambara, H.; Ueda, T.; Kuchitsu, K. *J. Chem. Phys.* **1987**, *86*, 6018.
(22) Egawa, T.; Yamamoto, S.; Ueda, T.; Kuchitsu, K. *J. Mol. Spectrosc.* **1987**, *126*, 231.
(23) Glendening, E. D.; Halpern, A. M. *J. Phys. Chem. A* **2005**, *109*, 635.
(24) Blake, T. A.; Xantheas, S. S. *J. Phys. Chem. A* **2006**, *110*, 10487.
(25) Dunitz, J. D.; Schomaker, V. *J. Chem. Phys.* **1952**, *20*, 1703.
(26) Almenningen, A.; Skancke, P. P. N.; Bastiansen, O. *Acta Chem. Scand.* **1961**, *15*, 711.
(27) Lord, R. C.; Stoicheff, B. P. *Can. J. Phys.* **1962**, *40*, 725.
(28) Ueda, T.; Shimanouchi, T. *J. Chem. Phys.* **1968**, *49*, 470.
(29) Egawa, T.; Yamamoto, S.; Kuchitsu, K. *J. Mol. Spectrosc.* **1988**, *129*, 72.
(30) Vogelsanger, B.; Caminati, W.; Bauder, A. *Chem. Phys. Lett.* **1987**, *141*, 245.
(31) Caminati, W.; Vogelsanger, B.; Meyer, R.; Grassi, G.; Bauder, A. *J. Mol. Spectrosc.* **1988**, *131*, 172.
(32) Malloy, T. B. J.; Lafferty, W. J. *J. Mol. Spectrosc.* **1985**, *54*, 20.
(33) Li, H.; Cameron, C.; Philips, L. A. *J. Chem. Phys.* **1994**, *100*, 8590.
(34) Roberts, J. D.; Sauer, C. W. *J. Am. Chem. Soc.* **1949**, *71*, 3925.
(35) Shen, Y. R. *The Principles of Nonlinear Optics*; John Wiley & Sons: 1984.
(36) Mukamel, S. *Principles of Nonlinear Spectroscopy*; Oxford University Press: New York, 1995.
(37) Grimberg, B. I.; Lozovoy, V.; Dantus, M.; Mukamel, S. *J. Phys. Chem. A* **2002**, *106*, 697.
(38) Burenin, A. V. *Opt. Spectrosc.* **2004**, *97*, 860.
(39) Weber, A. *J. Chem. Phys.* **1980**, *73*, 3952.
(40) Hegelund, F.; Rasmussen, F.; Brodersen, S. *J. Raman Spectrosc.* **1973**, *1*, 433.
(41) Brodersen, S. High Resolution Raman Spectroscopy of Gases. In *Raman Spectroscopy*; Weber, A., Ed.; Springer: Berlin, 1978.
(42) Polanyi, J.; Woodall, K. *J. Chem. Phys.* **1971**, *56*, 1563.
(43) Procaccia, I.; Levine, R. *J. Chem. Phys.* **1975**, *63*, 4261.
(44) Bak, K. L.; Gauss, J.; Jorgensen, P.; Olsen, J.; Helgaker, T.; Stanton, J. F. *J. Chem. Phys.* **2001**, *114*, 6548.
(45) Pawlowski, F.; Jorgensen, P.; Olsen, J.; Hegelund, F.; Helgaker, T.; Gauss, J.; Bak, K. L.; Stanton, J. F. *J. Chem. Phys.* **2002**, *116*, 6482.
(46) Barone, V. *J. Chem. Phys.* **2005**, *122*, 014108.
(47) Champion, R.; Godfrey, P. D.; Bettens, F. L. *J. Mol. Spectrosc.* **1978**, *155*, 18.